

Seismic design for enhanced building performance using rocking steel braced frames



Michael Pollino

Dept. of Civil Engineering, Case Western Reserve University, Bingham Bldg. Room 208, 10900 Euclid Ave, Cleveland, OH 44106, United States

ARTICLE INFO

Article history:

Received 12 December 2013

Revised 15 May 2014

Accepted 3 November 2014

Available online 22 November 2014

Keywords:

Seismic

Rocking

Steel

Braced frame

Self-centering

Residual drift

Seismic performance

Floor acceleration

Analysis

ABSTRACT

Performance-based seismic design has brought about innovative rocking and self-centering structural systems such as rocking steel braced frames (RBF). This lateral force resisting system has recently received focused attention in academic research however has seen limited application in practice to date. This may be due in part to the unconventional load path, plastic mechanisms, and unique dynamic characteristics of the system. The transfer of forces through a RBF with passive energy dissipating devices (steel yielding and viscous) is described and a simplified approach proposed to quantify peak dynamic deformation and force response. Enhanced performance can be achieved by including viscous damping devices over hysteretic devices and post-tensioning (proposed in previous research). The dynamic response of RBF are evaluated through nonlinear transient finite element seismic analyses with ground motion sets. Additionally, the demands placed on non-structural components contained on each building floor was investigated through the computational model by calculating critical response quantities such as inter-story drift, peak floor acceleration, and floor spectra. Structural and non-structural demands are compared with a buckling-restrained braced frame (BRBF) to illustrate the differences in seismic behavior and potential benefits of a well-designed rocking steel braced frame.

© 2014 Elsevier Ltd. All rights reserved.

1. Introduction

Rocking braced frames (RBF) are a new, developing seismic lateral force resisting system capable of enhanced seismic performance that can minimize or prevent damage to structural components, re-center following an earthquake event, and potentially limit demands on non-structural components. The primary structural components (beams, columns, braces) are designed to remain elastic while passive energy dissipating devices are implemented at the uplifting location to control the response. The RBF system investigated in this paper utilizes both steel yielding and viscous damping devices in parallel for response control. While well-designed conventional ductile steel seismic systems (SCBF, EBF, BRBF, etc.) perform adequately from a life-safety standpoint, damage and residual drift imparted on a structure even in a design basis earthquake might require extensive repairs or demolition following the earthquake.

The behavior and design of a 3-story RBF building including both primary rocking mode and higher mode response are discussed. The forces generated from higher mode response can be significantly larger than the forces to form the 1st mode rocking

plastic mechanism but must be accounted for to ensure elastic frame response. Additionally, the higher mode response has significant impact on the floor spectra. Nonlinear transient analysis is performed to calculate response for three sets of 10 ground motions representing far-field DBE and MCE and near-field events at a southern California site.

This paper discusses the behavior and a seismic design approach for rocking steel braced frame buildings and advances knowledge on this next-generation seismic LFRS by: (i) investigating behavior of a more beneficial combination of passive energy dissipating devices that can eliminate the need for post-tensioning, (ii) proposes a design approach to predict both dynamic deformations and force response including higher mode effects, (iii) quantifies demands on both structural and non-structural components, and (iv) compares RBF performance with a similarly designed BRBF building.

2. Background

Seismic steel lateral force resisting systems (LFRS) for building structures currently adopted in the AISC Seismic Design Provisions [1] have been developed with the intent of allowing structural damage even under design-basis seismic events. All current

E-mail address: mcp70@case.edu

seismic steel LFRS use a design approach that sizes protected zones for forces below the elastic force level by accounting for the actual overstrength and ductility of the LFRS and then sizes all surrounding non-protected zones for the ultimate force of the protected zone, a capacity design approach. From a life-safety standpoint, this may provide acceptable structural response. However, from an economic, operational, and sustainability standpoint the behavior is undesirable since damage in the protected zones requires costly repairs of the protected zone members and likely also of the surrounding members, connections, and floor slabs. Additionally, the plastic deformations induced on the protected zones results in permanent deformations and residual drift in the structural system following an earthquake.

A structural system that allows a braced frame or wall to uplift and rock can potentially provide damage-resistant behavior with enhanced performance and can provide a restoring force mechanism through gravity loads and/or post-tensioning forces capable of self-centering (eliminating residual drift). Energy dissipating devices can then be added to control the rocking response to within allowable limits. The performance of this next-generation LFRS is much improved from currently adopted seismic steel LFRS however further investigation of system level structural response, implementation details, and development of analysis and design tools amenable to implementation in practice are needed to advance these systems into common practice. Additionally, the demands placed on non-structural components using these seismic systems need to be assessed for operationally critical structures. Non-structural components may be sensitive to both deformations and floor accelerations therefore it is desirable to control both of these response quantities to limit damage.

Others ([2–4]) have investigated behavior of rocking steel braced building frames that incorporate vertical post-tensioning strands attached to the rocking braced frame that adds to the restoring force provided by the tributary gravity load carried by the frame and increases the total lateral force resistance of the frame. The post-tensioning strands add large concentrated forces that must be adequately distributed to the frame. Either steel yielding devices or friction devices are incorporated along the height of uplifting columns to dissipate seismic energy. The systems developed the expected response through analytical and experimental verification which focused on displacements and forces. Roke et al. [4] observed that the member forces can be significantly affected not only by the rocking mode response but also by the higher mode effects and developed a set of load factors through probabilistic analysis for the 6-story building and suite of seismic ground motions used in that study. Weibe [5] proposed the inclusion of multiple rocking sections along a wall's height to reduce the demands caused by higher mode force effects in a multi-story building. The approach was shown to reduce force demands from the higher mode effects although requires additional rocking connection details between sections.

Tremblay et al. [6] have investigated a similar rocking braced frame concept for seismic resistance of building structures but have investigated implementation of nonlinear fluid viscous dampers as the energy dissipation device at the base of the rocking frame column. Shake table testing and analytical studies were performed to evaluate and verify response.

Gunay et al. [7] evaluated the use of rocking concrete walls to create a rigid core to attract seismic forces and limit demands on non-ductile framing potentially preventing soft story failures. The rocking wall rehabilitation approach for non-ductile moment frame structures was shown to be cost effective with minimal construction complexity providing potential benefit for developing countries. Pollino et al. [8] proposed a similar rehabilitation technique for sub-standard steel framing utilizing large pin-supported steel columns or trusses.

Pollino and Bruneau [9] investigated a rocking system for the seismic design or retrofit of steel truss bridge piers. The piers represented an essentially SDOF system and was investigated both analytically (using nonlinear transient analyses) and experimentally (using large-scale 6DOF shaking table testing). The restoring force was supplied strictly by the vertical tributary weight in this application. The dynamic behavior of bridge piers is also fundamentally different from that of buildings due to the participation of higher lateral modes in the seismic response of buildings.

Kam et al. [10] investigated the use of various combinations of yielding, friction, and viscous passive energy dissipation devices in series or in parallel for achieving enhanced damage-free performance for structures located in both far-field and near-field earthquakes. The concept was investigated numerically using simple SDOF models.

Other self-centering steel seismic lateral force resisting systems have been proposed in recent years that include post-tensioned moment frames ([11–13], among others) and re-centering bracing devices ([14–16]). While these systems have similar self-centering hysteretic behavior, they generally do not experience the higher mode effects described in this paper which result from the continuous elastic frame introduced over the building height with the rocking braced frame.

3. Rocking braced frame behavior

The rocking braced frame (RBF) seismic lateral force resisting system described here (illustrated in Fig. 1) consists of an elastic braced frame within a building frame which is allowed to uplift from its supports (sliding prevented) prior to diagonal brace yielding and buckling. The frame may or may not be post-tensioned vertically to provide a vertical restoring force (F_{PT}) in addition to the tributary vertical weight (w_D). The static force–deformation behavior of a RBF with displacement-based steel yielding devices (SYD) and post-tensioning has been formulated and described in detail by others [2]. The proposed seismic system described here includes both displacement-based steel yielding devices (SYD) and velocity dependent viscous dampers (VD) implemented at the uplifting location to control the response. The steel yielding devices are considered to provide displacement-based hysteretic behavior with kinematic and isotropic material hardening. The viscous dampers considered have a force output based on:

$$F_{VD} = c_d \cdot \text{sgn}(v_d) \cdot (|v_d|)^{\alpha_d} \quad (1)$$

where c_d = damping constant, v_d = relative velocity across damper ends, and α_d = damping exponent. The addition of viscous damping

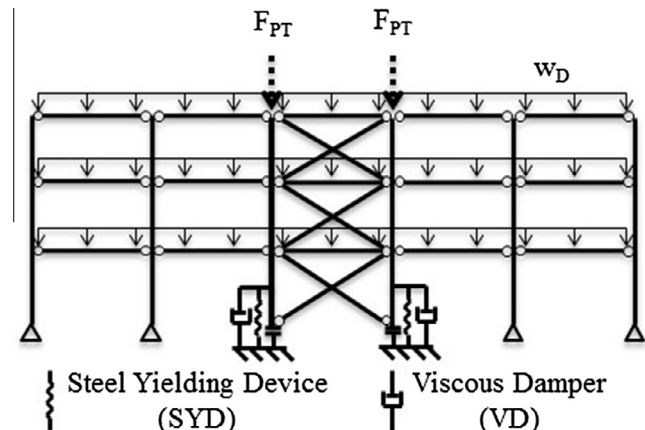


Fig. 1. RBF frame illustration.

(VD) devices provides enhanced system performance without impacting the self-centering capability of the frame. Since the self-centering can occur “slowly” following an earthquake, the velocity-dependent force output from the VD does not impact the frames ability to self-center. The displacement dependent force–displacement behavior of the SYD will affect self-centering of a RBF and requires an adequate restoring force provided by the tributary weight to the RBF columns plus the frame post-tensioning (if needed). This puts an upper limit on the yield force of the SYD equal to the vertical tributary weight plus the applied post-tensioning force.

3.1. Nonlinear static backbone curve

Prior to uplift of the braced bay leg, the elastic behavior is very similar to that of a conventional braced frame with elastic lateral stiffness, k_o . Post-uplift, the frame flexibility increases and an upward force is applied to the SYD. After uplift of the frame (decompression of a leg), the lateral stiffness of the frame is equal to:

$$k_r = \left[\frac{1}{k_o} + \frac{1}{(k_{SYD} + k_{PT}) \cdot \left(\frac{d}{H}\right)^2} \right]^{-1} \quad (2)$$

where k_o = initial braced frame lateral stiffness, k_{SYD} = vertical stiffness of the steel yielding device, k_{PT} = axial stiffness of the vertically oriented post-tensioning strands (if present), d = braced frame width, and H = height of RBF. As the lateral forces are increased, the steel yielding device will yield and the system post-yield lateral stiffness (k_{PY}) reduces to:

$$k_{PY} = \left[\frac{1}{k_o} + \frac{1}{(k_{PT} + \alpha \cdot k_{SYD}) \cdot \left(\frac{d}{H}\right)^2} \right]^{-1} \quad (3)$$

where α = post-yield stiffness ratio for the steel yielding device and all other parameters have been defined previously. At yield of the SYD, the lateral base shear force (V_y) considering an inverted triangular acceleration distribution and equal story heights and weights is equal to:

$$\begin{aligned} V_y &= \frac{3}{7} \cdot (P_v + F_{SYD} + F_{PT} + 2 \cdot k_{PT} \cdot \Delta_{ySYD}) \cdot \frac{d}{h} \\ &= \frac{3}{7} \cdot P_v \cdot (1 + \eta_L + \eta_{LPT} + 2 \cdot k_{PT} \cdot \Delta_{ySYD}) \cdot \frac{d}{h} \end{aligned} \quad (4)$$

where P_v = vertical tributary weight to a rocking braced frame column, F_{SYD} = yield force of the SYD, F_{PT} = initial post-tensioning force on a rocking braced frame column, Δ_{ySYD} = yield displacement of the SYD, and h = story height. Normalizing the SYD yield strength and initial post-tensioning force to the vertical tributary weight results in parameters η_L and η_{LPT} respectively and a lateral base shear force shown by the second expression in Eq. (4). Note that a SYD strength ratio, η_L , less than $1 + \eta_{LPT}$ is required to provide system self-centering. Although others [17] have proposed that restoring forces less than this value (based strictly on static equilibrium) would likely result in minimal residual drift due to the dynamic nature of the earthquake.

The general static lateral force–deformation behavior of the system is shown in Fig. 2 (focusing on the case with $\eta_L = 0$ and $\eta_L = 0.67$). Without post-tensioning strands and SYD, the system exhibits a nonlinear-elastic (rocking) behavior seen in Fig. 2 (line with $\eta_L = 0$) and has no post-yield stiffness (see Eq. (3)). For RBF buildings designed for reasonable levels of drift (1.5%), P – Δ effects could be neglected.

After an inelastic deformation of the SYD greater than $2 \Delta_{ySYD}$, the frame reverses direction and the SYD will yield in the reverse direction until it comes back into contact with the support. This

changes the static hysteretic behavior by transitioning to the system rocking stiffness (Eq. (2)) at a lower level of lateral load (see Fig. 2b) due to the fact that some of the gravity load and post-tensioning force is transferred into the SYD after an initial yielding cycle. For a SYD yield strength equal to the vertical gravity load and post-tensioning force, the system will effectively have an initial elastic stiffness equal to k_r for the remaining cycles.

3.2. Dynamic hysteretic behavior

Including the SYD and VD and considering dynamic, harmonic horizontal motion of the RBF system would result in the additional hysteretic behavior curves shown in Fig. 2. For this illustration, the VD has various sizes ($\eta_{LV} = 0.33, 0.67, 1.33, 2.67$) however the SYD strength is held constant ($\eta_L = 0.67$). The damper size (η_{LV}) is determined by the force output at peak system velocity (zero-displacement assuming harmonic response) with an effective system period of vibration equal to 1.7 s. and peak drift of 1.5% (values calculated for a prototype RBF building later). The behavior is similar to the static behavior but the additional force provided by the VD changes the hysteretic behavior as shown. Similar to the SYD and PT force, the VD peak force output is expressed normalized by the vertical tributary RBF column force by η_{LV} .

4. Design of rocking braced frame drift and self-centering

The design of a RBF requires understanding of the static and dynamic nonlinear hysteretic behavior of the system along with the elastic dynamic higher mode effects. The design must consider drift control, strength design of the rocking braced frame to prevent inelastic behavior (damage), and potentially braced frame stiffness to control floor accelerations (discussed later). Since the RBF includes passive hysteretic and viscous dampers, a ductile based design methodology is not sufficient and design methods that account for the contribution of the devices must be considered. An approach for sizing the SYD and VD to achieve a target drift and capacity protection of the rocking braced frame is presented.

4.1. Prototype building considered in study

The design of a RBF is illustrated here for a 3-story building with plan dimensions of 30.5 m by 48.8 m, bay widths of 6.1 m, story height of 3.96 m, and seismic floor weights of 10.8 kN/m² was selected for the study. Seismic response parallel to the 30.5 m dimension is considered with a frame similar to that shown in Fig. 1. The building is assumed to be located at a southern California site with design spectral acceleration values of $S_{D5} = 1.0$ g and $S_{D1} = 0.69$ g.

4.2. Prediction of RBF displacements and sizing SYD, VD, and PT

In order to predict peak system deformations, the response spectrum analysis procedure for structures with damping systems from ASCE 7-10 [18] Section 18.4 is used. The procedure essentially produces an equivalent linear-viscous system to calculate a spectral displacement from the site design spectrum. The procedure requires calculation of the nonlinear static force–deformation behavior of the structure (or calculation of base shear force at design displacement), site seismicity, modal properties, and energy dissipation capacity. An effective system period (T_D) is calculated at the design displacement (Δ_D) as:

$$T_D = 2 \cdot \pi \cdot \sqrt{\frac{W_1}{g \cdot k_{effD}}} \quad (5)$$

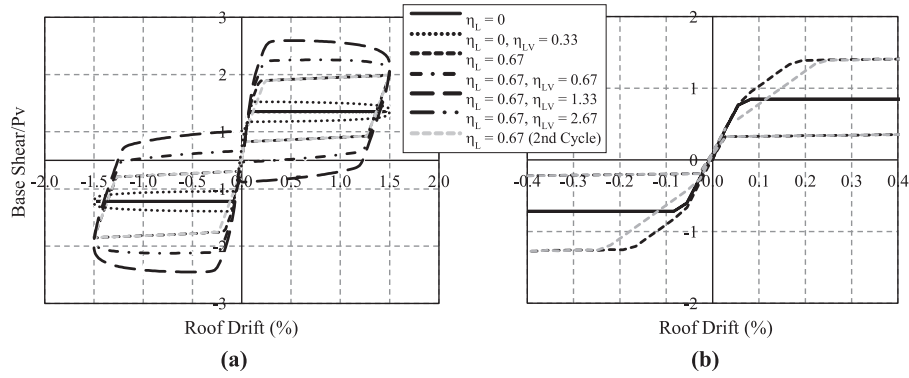


Fig. 2. Hysteretic behavior of rocking braced frame system (a) various combinations of steel yielding device and viscous damper sizes and (b) 2nd cycle behavior of system with steel yielding devices.

where W_1 = the effective first mode weight and k_{effD} could be estimated as V_y/Δ_D . The total equivalent damping (β) in the 1st mode (rocking) at the design displacement is equal to:

$$\beta = \beta_I + \beta_{SYD} + \beta_{VD} \tag{6}$$

where β_I = inherent damping (2% assumed), β_{SYD} = hysteretic damping provided by steel yielding device, and β_{VD} = damping provided by viscous damper. Effective damping provided by the SYD is calculated by:

$$\beta_{SYD} = q_H \cdot (0.64 - \beta_I) \cdot \left(1 - \frac{1}{\mu_D}\right) \tag{7}$$

where $\mu_D = \Delta_D/\Delta_y$. For systems which have a SYD strength greater than the PT strength but less than the combined PT and tributary gravity load ($\eta_L < \eta_L < 1 + \eta_{LPT}$), q_H represents the fraction of energy dissipated per cycle by the SYD compared to that of a bi-linear hysteretic system and is defined by:

$$q_H = \frac{\eta_L - \eta_{LPT}}{1 + (\eta_L - \eta_{LPT})} \tag{8}$$

This range of SYD strength is practical since $\eta_L < 1 + \eta_{LPT}$ is needed to provide system self-centering and $\eta_L > \eta_{LPT}$ provides SYD strength (energy dissipation) greater than PT strength (elastic strain energy) which is more desirable. The effective damping provided by the VD is:

$$\beta_{VD} = \frac{W_D}{4 \cdot \pi \cdot U_D} \tag{9}$$

where:

$$U_D = \frac{1}{2} \cdot k_{effD} \cdot \Delta_D^2 \tag{10}$$

$$W_D = \left(\frac{2 \cdot \pi}{T_D}\right)^{\alpha_d} \cdot c_d \cdot \lambda_d \cdot [\Delta_{upLD}^{\alpha_d+1}] \tag{11}$$

where W_D is the work done by a nonlinear viscous damper undergoing a cycle of harmonic motion at the design level of deformation (Δ_D) as derived in [19] with:

$$\lambda_d = 4 \cdot (2^{\alpha_d}) \cdot \frac{(\Gamma(1 + \frac{\alpha_d}{2}))^2}{\Gamma(2 + \alpha_d)} \tag{12}$$

The stroke on the damper is equal to the uplifting displacement of the RBF column (Δ_{upLD}) and can be estimated by:

$$\Delta_{upLD} = \left[\Delta_D - \frac{P_v \cdot (1 + \eta_L + \eta_{LPT}) \cdot \frac{d}{H}}{k_o} \right] \cdot \frac{d}{H} \tag{13}$$

Based on the effective period from Eq. (5) and the effective damping from Eq. (6), the system displacement can be predicted

by calculating the spectral displacement of this equivalent linear-viscous system with a spectrum reduced by factors for the effective damping (provided in [18]).

4.3. Capacity design of RBF

A method for combination of force effects is proposed based on response during the primary rocking mode and an appropriate modal combination rule for inclusion of higher mode effects.

4.3.1. Rocking mode forces

Calculation of peak member forces in the rocking mode includes static forces required to develop the plastic yield mechanism (Fig. 3a with system at peak deformation) and the viscous damper forces at peak velocity (Fig. 3b). Consistent with the ASCE 7–10 procedure, the peak damper force output is added to the plastic mechanism forces (as seen in Fig. 3b) due to the large system ductility expected with a RBF which suggest that the system is approximately at peak velocity (peak VD force) following yield of SYD. All internal forces developed based solely on the rocking lateral response can be determined from the free-body diagram shown in Fig. 3b.

4.3.2. Higher mode forces

The impact of higher lateral mode effects on rocking systems has been noted by past researchers [4] and the additional forces

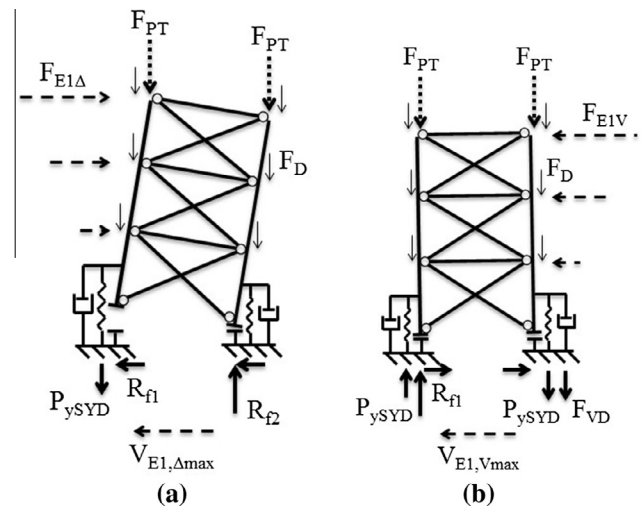


Fig. 3. Free-body diagram of RBF including rocking mode forces at (a) maximum displacement and (b) nearly maximum velocity.

must be accounted for to design RBF primary members to remain elastic. The effects of higher modes are more significant for the RBF system compared to conventional ductile systems due to the elastic structural behavior above the rocking interface. The plastic mechanism shape for RBF system is such that it does not significantly restrain first mode behavior however the continuous elastic RBF does restrain higher mode shapes while ideally not allowing any yielding along the height of the building. Thus the first mode has a force limiting mechanism provided by the base overturning moment however the higher modes are restrained by the elastic RBF. Such higher mode effects have also been noted in flexural yielding reinforced concrete walls where a concentrated plastic hinge forms at the base of the wall and a continuous elastic body extends over the height of the building. The rocking plastic mechanism limits the forces that can develop in a 1st mode deformation however 2nd and higher mode deformations cause large elastic forces to build-up in the frame. Conventional ductile systems which implement yielding mechanisms along building height provide however a means for limiting forces in the higher modes.

The higher mode force effects can be calculated from elastic modal force vectors [20] as:

$$F_{i,m} = w_{F_i} \cdot (\phi_m)_i \cdot \frac{\Gamma_m}{W_m} \cdot V_m \quad (14)$$

where w_{F_i} = floor weight i , ϕ_m = shape of mode m , Γ_m = modal participation factor, W_m = effective modal weight, and V_m = modal base shear force defined by:

$$V_m = C_{sm} \cdot W_m \quad (15)$$

where C_{sm} = seismic response coefficient determined at the period of mode m .

4.3.3. Combined total force effects

The higher modes have an equivalent damping limited to the frame inherent damping (2%). Considering an X-braced rocking frame and using a SRSS modal combination of the higher modes results in a braced frame diagonal force in story j (F_{brj}) of:

$$F_{brj} = \frac{\sum_{i=j}^3 P_{s_i}}{2 \cdot \cos(\theta_{br})} + \frac{\eta_{LV} \cdot P_v}{2 \cdot n \cdot \sin(\theta_{br})} + \sqrt{\sum_{m=2}^3 \left(\frac{\sum_{i=j}^3 F_{i,m}}{2 \cdot \cos(\theta_{br})} \right)^2} \quad (16)$$

where P_s = lateral floor inertia force at yield in the rocking mode and θ_{br} = brace angle. The higher mode diagonal brace forces can easily be two to three times the force required for the plastic rocking mechanism in the 1st mode. Column forces tend to be impacted less by higher modes due the opposing higher mode shears consistent with the higher mode shapes however must still be accounted for and the column forces could be similarly determined by adding the rocking mode forces with the SRSS of the higher mode demands. The total column force in story j (F_{cj}) is proposed to be calculated as follows:

$$F_{cj} = (n + 1 - j) \cdot \left(\frac{P_v}{n} \right) + \sum_{i=j}^3 \left[P_{s_i} \cdot \frac{(i - j + 1) \cdot h}{d} \right] + \eta_{LV} \cdot P_v \cdot \left(\frac{1 + n - j}{3} \right) + \sqrt{\sum_{m=2}^3 \left[\sum_{i=j}^3 \left[F_{i,m} \cdot \frac{(i - j + 1) \cdot h}{d} \right] \right]^2} \quad (17)$$

The column force calculation assumes that the frame will have formed the plastic rocking mechanism while the 2nd and 3rd modes are combined with an SRSS modal combination rule. In some cases a CQC modal combination rule may be more appropriate.

4.4. Sample prototype building RBF designs

The proposed simplified design approach was used to generate a set of potential designs with a target drift of 1.5%. A secondary design objective was to limit the base shear force at the design displacement to reduce member forces and floor accelerations. A number of lateral force resisting frames (n_f) and rocking frame aspect ratio (H/d) were considered in the prototype building described previously and then the required post-tensioning, steel yielding device, and viscous damper strengths required to achieve the target drift of 1.5% were determined. The resulting designs are provided in Table 1. The VD strength ratio (η_{LV}) was limited to 2.5 for practical considerations of damper sizes. Post-tensioning is not required for cases with smaller rocking frame aspect ratios (H/d) and using 4 or more lateral force resisting frames (n_f). The RBF design in bold in Table 1 is selected for further study since it had desirable response characteristics ($\sim 1.5\%$ drift, minimum base shear, no post-tensioning required).

Table 1
RBF designs.

n_f	H/d	H (m)	d (m)	η_{LPT}	A_{PT} (cm ²)	η_L	A_{SYD} (cm ²)	η_{LV}	T_{eff} (s)	$P(\Delta_D)/W$	β (%)	Drift _D (%)	Δ_{upLD} (cm)	F_c (kN)	F_{br} (kN)
4	2.0	11.9	6.1	0	0	1.0	32	2.5	1.7	0.13	63	1.58	8.97	5698	2767
2	2.0	11.9	6.1	2.0	18.7	3.0	103	2.5	1.2	0.26	35	1.47	8.76	13,024	6819
8	2.0	11.9	6.1	0.0	0	0.8	26	0.0	1.3	0.23	24	1.49	8.97	3350	1432
4	3.9	11.9	3.0	1.3	11.6	2.3	77	2.5	1.5	0.17	42	1.50	4.50	9564	3754
2	3.9	11.9	3.0	4.5	41.3	5.5	194	2.5	1.3	0.22	32	1.52	4.42	19,541	8065
4	7.8	11.9	1.5	3.5	32.3	4.5	155	2.5	1.6	0.16	35	1.50	2.26	15,458	5912
2	7.8	11.9	1.5	10.0	92.3	11	381	2.5	1.4	0.20	30	1.53	2.21	33,433	12,780

Based on ASCE 7 Section 18.4 (response spectrum procedure for structures with damping systems). Values in bold are RBF design shown considered throughout paper.

Table 2
Modal properties of RBF and BRBF systems considered in study.

Frame design	Frequencies (Hz)				Participation weight/total			Participation factors		
	f_1 (fixed base)	f_1 (rocking)	f_2	f_3	W_1	W_2	W_3	Γ_1	Γ_2	Γ_3
RBF – strength design	2.01	1.00	5.70	7.66	0.84	0.13	0.01	2.43	0.95	0.24
RBF – 2X stiffness	2.78	1.06	7.84	10.4	0.86	0.13	0.01	2.45	0.96	0.25
RBF – 4X stiffness	3.75	1.09	10.6	13.9	0.88	0.13	0.01	2.48	0.97	0.25
RBF – 1000X stiffness	–	1.16	–	–	0.84	–	–	2.42	–	–
BRBF	1.69	–	4.00	5.57	0.83	0.14	0.02	2.41	1.00	0.36

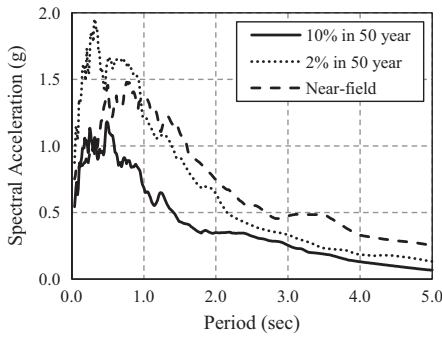


Fig. 4. Median spectra for each set of ten ground motions used in seismic transient analysis.

5. RBF building analytical model

The seismic response of the prototype building described above was calculated by performing nonlinear transient seismic analysis in the program ANSYS [21]. The model used nonlinear fiber beam

elements for all structural beams, columns, and braces however these elements were sized to remain elastic during seismic response using the equations presented previously. The steel yielding devices also used nonlinear beam elements to model a general nonlinear force deformation response which could reasonably represent a buckling-restrained brace [1], shear yielding panel [22], TADAS device [23], among others. A plasticity material model was used for beam elements that included kinematic hardening with steel properties consistent with ASTM A992 steel. The viscous damper was modeled using a uni-directional control element (Combin37 in ANSYS) that produces a force as a function of the relative velocity across the element nodes. The behavior assigned produced a force output based on the relative velocity raised to the 0.5 power to reflect the nonlinear force–velocity behavior as described by Eq. (1). The vertical support behavior at the base of the RBF columns was modeled with a gap-contact element (Combin40 in ANSYS) with stiffness in compression significantly larger than the axial stiffness of the column (rigid foundation) and no resistance to vertical uplift. The tributary horizontal and vertical masses were uniformly distributed along the beam lengths. The inherent damping of the system is included through a Rayleigh damping matrix

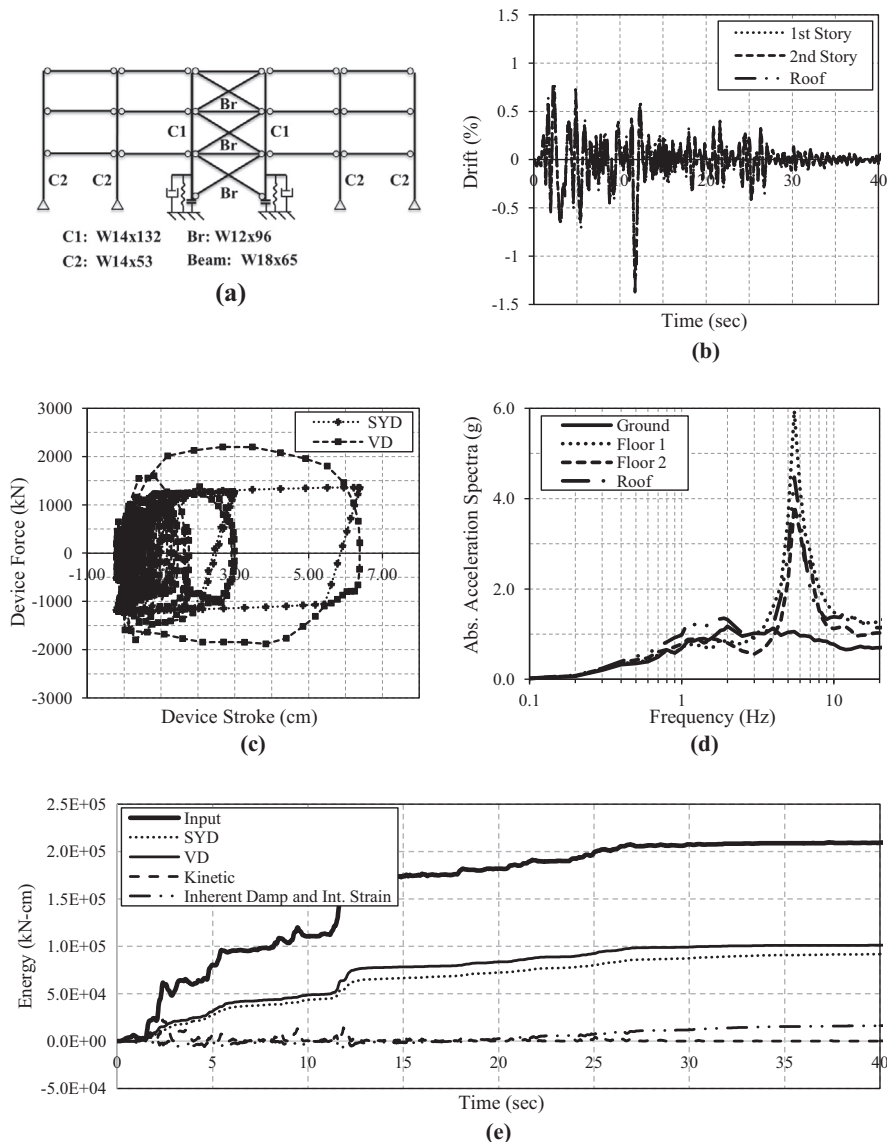


Fig. 5. Response RBF frame to LA01 ground motion (10% in 50 year hazard) (a) frame sections, (b) drift, (c) device hysteretic behavior, (d) floor spectra, and (e) system energy.

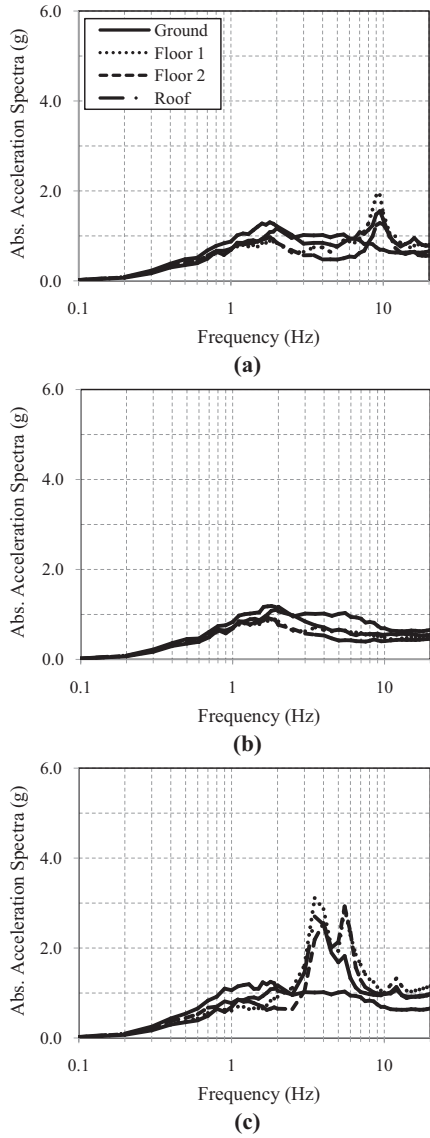


Fig. 6. Median RBF floor spectra, 10% in 50 year hazard level (a) 4X stiffness, (b) 1000X stiffness, and (c) yielding RBF braces.

by assigning 2% damping to the rocking mode and third mode with frequencies included in Table 2. Energy loss through inelastic collisions of the frame legs with the foundation are not explicitly modeled however the energy loss due to this mechanism is quite small compared to the energy dissipated by the SYD and VD elements.

Three sets of seismic ground motions which were originally generated for the SAC Steel project [24] were used in the analyses. Two sets of ten ground motions were for buildings at a Los Angeles, CA site for hazard levels of 10% and 2% in 50 year earthquake events and a set of ten near-field ground motions that include the fault-normal component with large velocity pulse are also considered. The median spectra for each set of ground motions are shown in Fig. 4. The statistical variability in the ground motions is expected to be represented of a southern California site.

A set of time history response of the RBF with properties noted in bold in Table 1 are shown in Fig. 5 for one of the ground motions at the 10% in 50 year hazard level that had a response spectrum which most closely matched the median spectrum around the

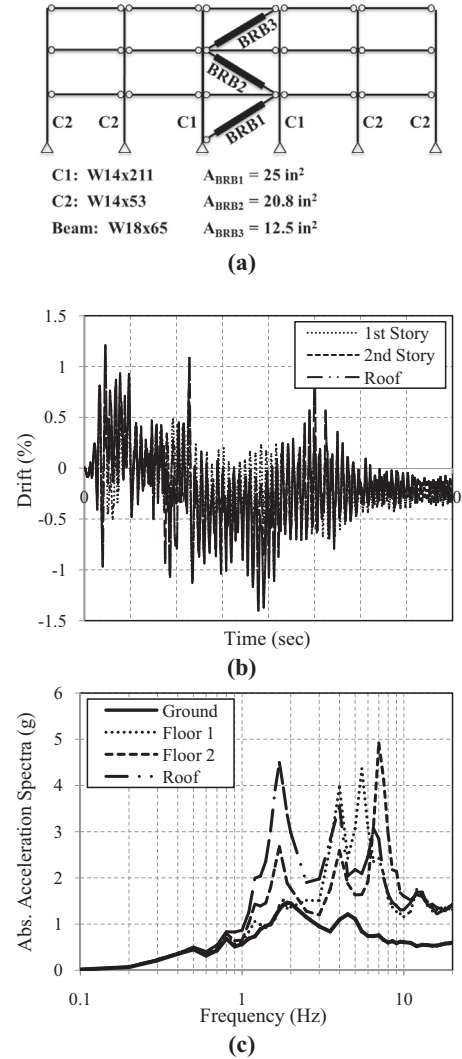


Fig. 7. Response BRBF frame to LA01 ground motion (10% in 50 year hazard) (a) frame and BRB sections, (b) drift, and (c) floor spectra.

rocking mode frequency (thus was expected to reasonably represent the set of motions). The 10% in 50 year motions had median spectral acceleration approximately matching the values considered for designs in Table 1. The frame drift shown in Fig. 5b is slightly less than the target drift of 1.5% calculated from the simplified analysis procedure from ASCE 7-10 (Table 1). Negligible drift exists at the end of the record due to the system self-centering ability. The force-deformation response of the SYD and VD are shown in Fig. 5c. The floor spectra are shown in Fig. 5d and significant spectral floor acceleration is observed at the frequency of the 2nd mode (5.7 Hz). The observed peak column force in the analysis was 6060 kN (slightly greater than the force predicted by Eq. (17), 5700 kN which is also noted in Table 1). Also, the peak diagonal brace force was equal to 2640 kN (less than the force predicted by Eq. (16), 2770 kN). In terms of both forces and deformations, the ASCE 7-10 procedure seems to predict the RBF response well. Additionally, the system energies were calculated (Fig. 5e) and it was observed for this record that the VD and SYD dissipated approximately 48% and 44% of the energy input from the ground shaking. The remaining 8% was dissipated through the inherent system damping.

5.1. Approaches for reducing RBF floor spectra response

Two potential approaches were investigated for controlling floor spectra response in a RBF: (i) increase the frame rigidity such that the frequencies of the higher modes lie outside the frequency range of the high energy content of the motions and (ii) to allow inelastic behavior of the bracing elements within the RBF at force levels greater than that to allow rocking to occur.

The first approach was investigated by running a series of cases increasing the cross-sectional area of the braced frame members by a factor of 4 and 1000 above the strength design required sizes and the resulting floor spectra are shown in Fig. 6. The case of 1000 times was simply included as a theoretical case of rigid behavior. The resulting modal properties of each RBF frame with varying rigidity are provided in Table 2. Increasing the RBF stiffness increases the “fixed-base” frame frequency however has little impact on the system “rocking” (post-uplift) frequency, as expected. Frequencies of the second and third modes are observed to increase quite significantly and this approach is effective at reducing floor spectra as evident in Fig. 6. Increasing the RBF member areas would increase cost of the RBF however could also significantly reduce the impact on non-structural components within the building.

The second approach for reducing floor spectra response introduced bi-linear hysteretic yielding elements as bracing members within the RBF however limited their strength to levels that allowed the RBF to uplift, yield the SYD, and transfer peak VD forces however were not designed to additionally include the

higher mode forces. Thus the diagonal members were designed for force levels according to Eq. (16) but without the final term which includes the higher mode force effects. The effect on floor spectra is shown in Fig. 6c where the peak floor spectral acceleration is approximately 3 g over a wider range of frequencies due to the yielding of the braces resulting in participation of some higher modes. While this approach is reasonably effective compared to the strength design system (Fig. 5d) but less effective than the stiffening approach (Fig. 6a and b), it would also require ductile detailing within the RBF.

5.2. BRBF model

In order to compare the response of a RBF system with a conventional ductile yielding lateral force resisting system, seismic analysis of the prototype building described above was performed with buckling-restrained braces implemented along the height. The buckling-restrained braced frame (BRBF) was designed with a target drift of 1.5% (same as for the RBF). The BRB sizes and frame member sizes are shown in Fig. 7. The BRB drift is seen in Fig. 7b to be slightly less than the 1.5% target drift however the frame also has a residual drift greater than 0.5% following ground shaking. The floor spectra shown in Fig. 7c is significant around the three BRBF modes (1.69, 4.0, and 5.57 Hz, see Table 2). The peak spectral value is similar to that of the RBF with strength designed frame stiffness however has large values over a much wider frequency range.

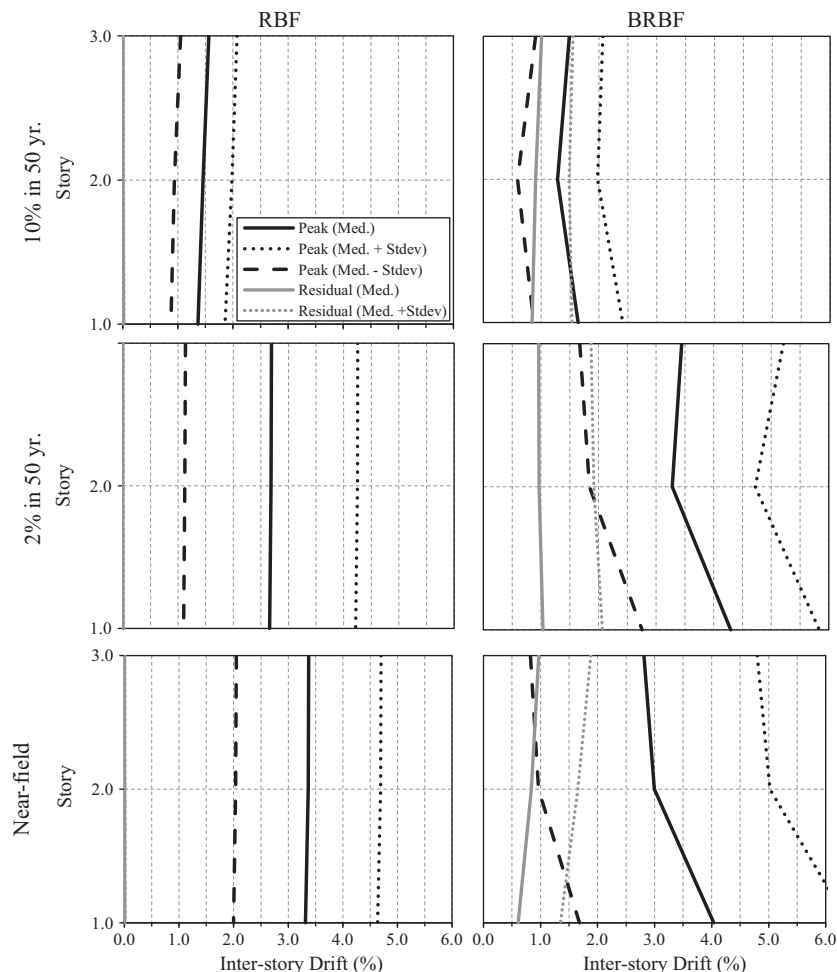


Fig. 8. Peak inter-story drift response of RBF and BRBF frame for each ground motion set.

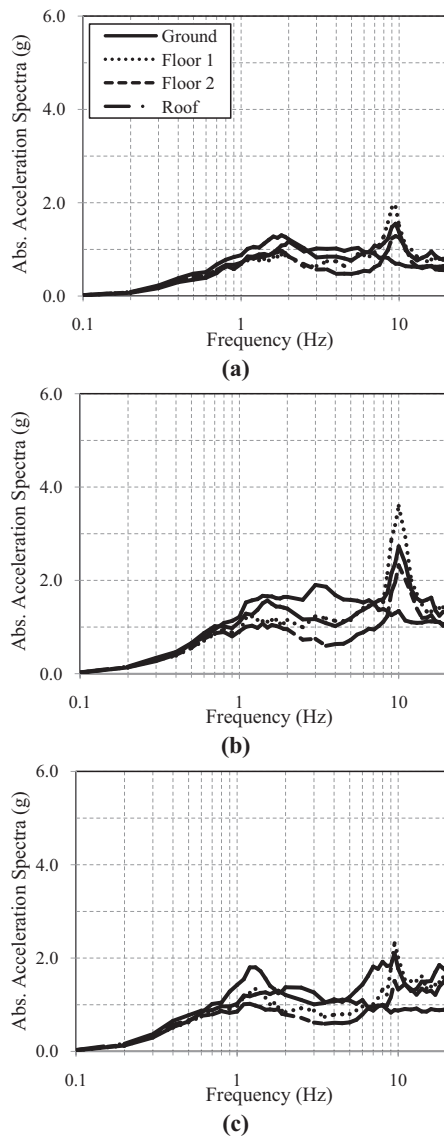


Fig. 9. Median RBF floor spectra for each ground motion set (a) 10% in 50 year, (b) 2% in 50 year and, (c) near-field.

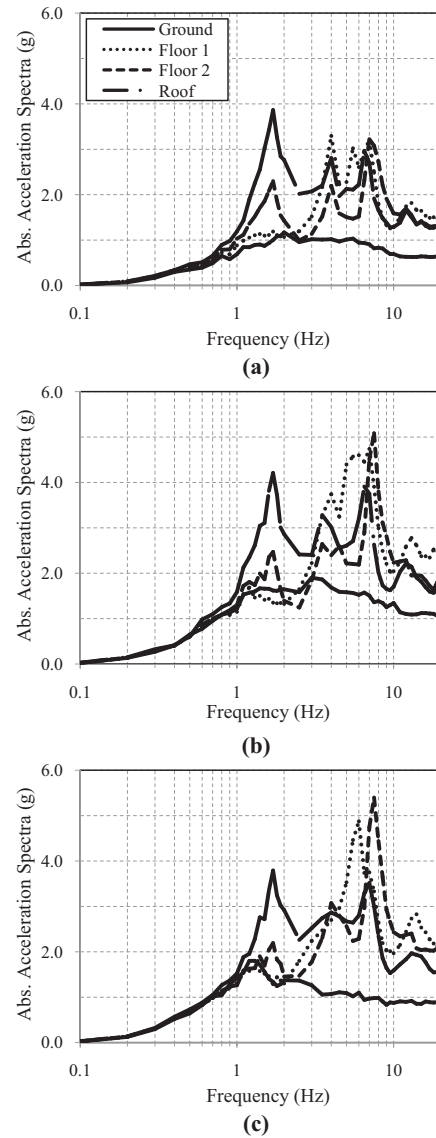


Fig. 10. Median BRBF floor spectra for each ground motion set (a) 10% in 50 year, (b) 2% in 50 year and, (c) near-field.

6. Transient analysis and results

The results of nonlinear transient analyses for each set of ground motions was performed and summarized in Figs. 8–10 and Table 3. The median RBF drift profile shown in Fig. 8 is nearly uniform regardless of the ground motion set due to the elastic braced frame over the building height that prevents concentrated drift in any one story. Both the RBF and BRBF drift in the 10% in 50 year hazard set is observed to be approximately 1.5% as this was the drift design objective. The RBF has slightly less variability in the drift response in the 10% in 50 y. set, similar variability in the 2% in 50 y. set, and significantly less variability in the near-field motion set. The BRBF has similar residual drift for all ground motion sets (approximately 1.0% median) while the RBF has essentially no residual drift for all cases (as expected).

The floor spectra for the 4X stiff RBF are shown in Fig. 9 for each set of ground motions. A significant spectral acceleration spike is observed at the RBF 2nd mode frequency of approximately 10 Hz (see Table 2) however floor spectral acceleration is observed to

be less than the ground input away from this modal frequency. The shape of the floor spectra is generally the same for each set of ground motions but the magnitude of the spectral acceleration at the 2nd mode frequency is larger for the 2% in 50 year motions as expected from the significantly larger spectral input around this frequency (Fig. 4). The BRBF floor spectra are shown in Fig. 10 and observed to be greater than the ground input spectra across almost all frequencies. Significant spikes in spectral acceleration are observed around all BRBF frame frequencies (see Table 2).

The RBF median peak brace and column axial forces are provided in Table 3 along with the BRBF median column axial force. The RBF median peak forces and variability (standard deviation of peak forces) are similar for the strength design frame and 4X stiff designed frame for each ground motion set however the forces are larger for the 2% in 50 year and near-field motions. The RBF and BRBF median peak column axial forces are generally similar for all ground motion sets however the variability in the BRBF column forces is significantly less likely due to the limited force to yield all BRBs while the RBF column force is impacted by the VD with force output dependent on the velocity.

Table 3
Median peak transient analysis results of RBF and BRBF systems for each hazard level.

Hazard level	Frame design	Story	Drift (%)	Residual drift (%)	Floor acc (g)	Brace force (kN)	Column force (kN)
10% in 50 y	RBF – strength design	Story 3	1.56 (0.52)	0.00 (0.01)	0.82 (0.34)	1699 (672)	1468 (351)
		Story 2	1.44 (0.52)	0.01 (0.01)	0.72 (0.27)	1797 (294)	3679 (841)
		Story 1	1.38 (0.49)	0.01 (0.01)	0.89 (0.47)	3136 (654)	6050 (716)
	RBF – 4X stiffness	Story 3	1.25 (0.49)	0.00 (0.01)	0.53 (0.17)	1423 (445)	1477 (280)
		Story 2	1.24 (0.49)	0.00 (0.01)	0.38 (0.14)	1971 (320)	3963 (658)
		Story 1	1.21 (0.48)	0.01 (0.01)	0.53 (0.2)	2905 (529)	6655 (974)
	BRBF	Story 3	1.49 (0.58)	1.01 (0.54)	0.92 (0.18)	–	1797 (40)
		Story 2	1.28 (0.69)	0.9 (0.58)	0.84 (0.18)	–	4328 (129)
		Story 1	1.64 (0.77)	0.84 (0.69)	0.92 (0.31)	–	7460 (191)
2% in 50 y	RBF – strength design	Story 3	3.15 (1.65)	0.03 (0.06)	0.78 (0.36)	2122 (645)	1833 (343)
		Story 2	3.12 (1.66)	0.01 (0.06)	0.53 (0.36)	2264 (365)	4760 (712)
		Story 1	2.94 (1.65)	0.01 (0.03)	0.86 (0.53)	3848 (894)	7553 (925)
	RBF – 4X stiffness	Story 3	2.69 (1.56)	0 (0.01)	0.53 (0.18)	1966 (440)	2024 (525)
		Story 2	2.69 (1.56)	0 (0.01)	0.4 (0.13)	2705 (645)	5458 (1437)
		Story 1	2.66 (1.56)	0 (0.01)	0.51 (0.25)	4101 (1023)	9719 (2705)
	BRBF	Story 3	3.44 (1.77)	0.96 (0.91)	0.78 (0.23)	–	1855 (102)
		Story 2	3.28 (1.44)	0.97 (0.95)	0.76 (0.26)	–	4466 (222)
		Story 1	4.3 (1.54)	1.04 (1.03)	0.81 (0.37)	–	7713 (400)
Near fault motions	RBF – strength design	Story 3	3.64 (1.26)	0.01 (0.03)	1.01 (0.23)	1868 (436)	1770 (307)
		Story 2	3.59 (1.29)	0.01 (0.03)	0.85 (0.27)	2331 (343)	4826 (707)
		Story 1	3.43 (1.26)	0.02 (0.02)	0.93 (0.42)	3790 (707)	7642 (1272)
	RBF – 4X stiffness	Story 3	3.38 (1.33)	0 (0.01)	1.04 (0.28)	2104 (476)	2411 (520)
		Story 2	3.36 (1.33)	0 (0.01)	0.74 (0.23)	3034 (663)	6152 (1397)
		Story 1	3.32 (1.32)	0 (0.01)	0.79 (0.28)	4697 (832)	10,729 (2891)
	BRBF	Story 3	2.81 (1.99)	0.97 (0.91)	1.06 (0.11)	–	1819 (80)
		Story 2	2.99 (2.03)	0.84 (0.82)	1.32 (0.31)	–	4484 (276)
		Story 1	4.04 (2.36)	0.61 (0.74)	1.21 (0.34)	–	7460 (356)

Value in parentheses is standard deviation over ground motion bin.

7. Summary and conclusions

The rocking braced frame (RBF) seismic lateral force resisting system can potentially provide increased seismic performance both for structural and non-structural components compared to conventional ductile systems with limited damage and a re-centering capability. The inclusion of viscous damping devices in parallel with steel yielding devices can enhance performance without impacting the self-centering capability and without the need for elastic post-tensioning of frame columns. The behavior of this type of seismic structural system is presented for various combinations of steel yielding and viscous damping elements and key parameters defined which are used in a simplified analysis approach. The influence of higher mode forces is significant for this type of LFERS and an approach to calculate the forces along with the plastic mechanism and viscous damping forces is presented and shown to provide reliable prediction of forces for design. Nonlinear transient analyses of a RBF and BRBF building (both designed for 1.5% drift) are performed using three seismic ground motion sets representing two hazard levels of far-field records and a set of near-field records (30 records total). Floor spectra are quantified from the analyses and approaches for controlling floor spectra with the RBF are examined. The RBF building is shown to provide similar levels of peak drift, essentially no residual drift, and significantly reduced floor spectra compared with the BRBF building. More research is needed to assess performance for a larger range of parameters, evaluate details for deformation compatibility between the rocking frame and slab, and to develop practical connection details at the rocking location. Furthermore, this paper only describes the horizontal response of a prototype 2D frame and the 3D building behavior and response is needed.

Acknowledgements

The research reported in this paper was supported in part by the Dept. of Civil Engineering at Case Western Reserve University.

The author wishes to acknowledge the sponsor. However, any opinions, findings, conclusions, and recommendations presented in this paper are those of the author and do not necessarily reflect the views of the sponsor.

References

- [1] AISC. *Seismic provisions for structural steel buildings*. Chicago, IL: American Institute of Steel Construction; 2005.
- [2] Eatherton M, Hajjar J, Ma X, Krawinkler H, Deierlein G. Seismic design and behavior of steel frames with controlled rocking – Part I: Concepts and quasi-static subassembly testing. ASCE Structures Congress, Orlando, Florida, May 12–15; 2010.
- [3] Sause R, Ricles J, Roke D, Chancellor N, Gonner N. Large-scale experimental studies of damage-free self-centering concentrically-braced frame under seismic loading. Structures Congress, ASCE; May 2010.
- [4] Roke D, Sause R, Ricles J, Gonner N. Design concepts for damage-free seismic resistant self-centering steel concentrically-braced frames. In: 14th World conference on earthquake engineering, Beijing, China; October 2008.
- [5] Weibe L. Mitigation of higher mode effects in self-centering walls by using multiple rocking sections. MS Thesis, University of Pavia, Italy; April 2008.
- [6] Tremblay R, Poirier L, Bouaanani N, Leclerc M, Rene V, Fronteddu L, Rivest S. Innovative viscously damped rocking braced steel frames. In: 14th World conference on earthquake engineering, Beijing, China; October 2008.
- [7] Gunay S, Korolyk D, Mar D, Mosalam K, Rodgers J. Infill walls as a spine to enhance the seismic performance of non-ductile reinforced concrete frames. ATC & SEI conference on improving the seismic performance of existing buildings and other structures, ASCE; December 2009.
- [8] Pollino M, Sabzehzar S, Qu B, Mosqueda G. Research needs for seismic rehabilitation of sub-standard buildings using stiff rocking cores. ASCE Structures Congress, Pittsburgh, PA; May 2013.
- [9] Pollino M, Bruneau M. Seismic testing of a controlled rocking steel bridge pier with hysteretic and viscous energy dissipation devices. *J Struct Eng ASCE* 2010;136(12):1523–32.
- [10] Kam WY, Pampanin S, Carr AJ, Palermo A. Advanced flag-shape systems for high seismic performance including near-fault effects. New Zealand society of earthquake engineering conference; 2007.
- [11] Lin Y, Sause R, Ricles J. Seismic performance of steel self-centering, moment-resisting frame: hybrid simulations under design basis earthquake. *J Struct Eng* 2013;139(11):1823–32.
- [12] Christopoulos C, Filiatrault A, Uang CM, Folz B. Post-tensioned energy dissipating connections for moment-resisting steel frames. *J Struct Eng, ASCE* 2002;128(9):1111–20.
- [13] Chou CC, Chen JH. Seismic design and shake table tests of a steel post-tensioned self-centering moment frame with a slab accommodating frame expansion. *Earthquake Eng Struct Dynam* 2011;40(11):1241–61.

- [14] Christopoulos C, Tremblay R, Kim HJ, Lacerte M. Self-centering energy dissipative bracing system for the seismic resistance of structures: development and validation. *J Struct Eng, ASCE* 2008;134(1):96–107.
- [15] Miller DJ, Fahnestock LA, Eatherton MR. Behavior of self-centering buckling restrained braces. In: 7th Conference on behavior of steel structures in seismic area, Santiago, Chile; 2012.
- [16] Chou CC, Chen YC. Development and seismic performance of steel dual-core self-centering braces. In: 15th World conference on earthquake engineering, Lisbon, Portugal; 2012.
- [17] Eatherton M, Hajjar J. Residual drifts of self-centering systems including effects of ambient building resistance. *Earthquake Spectra* 2011;27(3):719–44.
- [18] American society of civil engineers. Minimum design loads for buildings and other structures: ASCE/SEI 7-10. ASCE, Reston, VA; 2010.
- [19] Constantinou MC, Symans MD. Experimental and analytical investigation of structures with supplemental fluid viscous dampers. Technical report NCEER-92-0032. Buffalo, NY: National Center for Earthquake Engineering Research, The State University of New York at Buffalo; 1992.
- [20] Clough RW, Penzien J. *Dynamics of structures*. New York: McGraw-Hill Inc.; 1975.
- [21] ANSYS® academic research, Release 14.0, Help system, Mechanical application user's guide, ANSYS Inc.
- [22] Zahrai SM, Bruneau M. Seismic retrofit of steel slab-on-girder bridges using ductile end-diaphragms. Report OCEERC 98-20. Ottawa, Canada: Ottawa Carleton Earthquake Engineering Research Centre; 1998.
- [23] Tsai KC, Chen HW, Hong CP, Su YF. Design of steel triangular plate energy absorbers for seismic-resistant construction. *Earthquake Spectra, EERI* 1993;9(3):505–28.
- [24] Somerville P. Development of ground motion time histories for phase 2 of the FEMA/SAC steel project. Report No. SAC/BD-97/04, SAC Joint Venture, Sacramento, CA; 1997.